Effect of grain boundaries on the magnetoresistance of magnetite

S. I. Rybchenko,[1,2] Y. Fujishiro,[1] H. Takagi,[1] and M. Awano[1]
[1]*National Institute of Advanced Industrial Science and Technology, 2268-1 Shimo-Shidami, Moriyama-ku, Nagoya 463-8687, Japan*
[2]*Institute for Solid State Physics, Russian Academy of Sciences, Chernogolovka, Moscow district, 142432 Russia*
(Received 10 January 2005; revised manuscript received 27 April 2005; published 17 August 2005)

The effects of grain boundary morphology and stoichiometry had been systematically examined to clarify the role of natural grain boundaries in magnetoresistance of magnetite $Fe_{3(1-\delta)}O_4$. We found that the excess resistance, caused by presence of the grain boundaries, is negligibly low in stoichiometric polycrystals. Accordingly, there was no grain boundary magnetoresistance detected in dense polycrystals. Moreover, the incorporation of grain boundaries was found to decrease the resistance of polycrystalline samples below the Verwey transition temperature. That was connected to the enhanced conductivity of grain boundaries appearing due to the local suppression of charge ordering. On the other hand, the essential negative magnetoresistance was detected in granular samples, exploring the point contact geometry for intergrain contacts. That magnetoresistance is characterized by large high-field component and appearance over a wide range of oxidation. It has been explained within the model of magnetically inhomogeneous grain boundary with the characteristic magnetic thickness of the order of exchange length. The magnetoresistance effect was connected to the spin-dependent scattering at the transition layers of magnetization formed around hard magnetic defects. The contraction of these transition layers by external magnetic field is supposed to provide the origin of the observed magnetoresistance. The analysis of appropriate microscopic scattering mechanisms reveals the important role of point defects in the spin-dependent scattering. The second magnetoresistance component was separated at highly oxidized grain boundaries and associated with tunneling transport across the isolating grain boundaries. Although the oxidation was shown to improve the isolating properties of natural grain boundaries, the performance of oxidized grain boundary as a tunneling barrier is still poor.

DOI: 10.1103/PhysRevB.72.054424 PACS number(s): 72.25.Mk, 72.25.−b, 73.40.−c, 75.47.−m

I. INTRODUCTION

Magnetoresistance (MR) effect has been one of the most widely studied topics in solid state physics in past decade.[1] Half-metallic ferromagnetic materials, characterized by the presence of an energy gap for one of the spin orientations at the Fermi level, have been a subject of the increased interest as 100% spin-polarized material. One of the more interesting from the point of possible application is magnetite Fe_3O_4, which is ordered in a ferrimagnetic structure below 580 °C. Band structure calculations have shown that magnetite has a gap in the majority spin band and there is no gap in minority spin band at the Fermi level.[2,3] About 80% negative value of spin polarization had been measured in spin-polarized photoemission experiments at E_F.[4] A number of results were published regarding the MR observation in different magnetite-based structures. The high-field negative specific MR response had been observed in a bulk single crystal in the close vicinity of Verwey transition (T_V=123 K).[5] The negative MR associated with intergrain transport has been reported for polycrystalline thin films,[6,7] powder compacts,[7] and point contact formed by single crystals.[8] The largest low-field (LF) MR value (defined at the field of technical saturation of magnetization) has been observed for the breaking contact of two small single crystals −75% at 70 Oe.[8] But in most cases the magnitude of MR is much smaller than it might be expected from the high spin polarization degree of conducting electrons. The spin-valve tunnel structures prepared with Fe_3O_4 active electrode/s also have been studied. The one group reported an essential LF MR,[9] whereas the others declared a negligible MR effect, despite the high crystalline quality of epitaxial-grown samples.[10]

The reason for low or nonrepeatable MR response in magnetite is still not clear. One of the most common suggestions is a special property of grain boundary (GB) and magnetite interface to other material, which is supposed to have the decreased spin polarization and/or frustrated spin alignment.[10] Thus, the interface properties of magnetite appear as a subject of key interest for the further understanding of spin transport in this material. The relating information is very poor. Even the conclusion about the natural GB resistance is not clear. The evidence for low GB resistance has been obtained on thin films.[6] But for thin films, it has been shown they naturally contain a high density of antiphase boundaries.[11] These defects modify strongly the transport and magnetic properties of magnetite,[12] masking the effect of natural GBs. The data from the bulk polycrystalline magnetite are very limited[13] and not specific to the GB properties.

Another important aspect, which is not usually discussed, is the stoichiometry. The oxidation of magnetite affects its conductive properties through variation of the Fe^{2+}/Fe^{3+} ratio and introduction of iron-ion vacancies, finally turning magnetite into a dielectric maghemite γ-Fe_2O_3. The effect of such perturbation of conductivity on magnetoresistance seems not to be examined thoroughly so far. On the other hand, it was shown that magnetite can be oxidized by air even at room temperature.[14] This property points to the practically unavoidable problem with control of local oxygen stoichiometry at magnetite surfaces and interfaces with other oxides, especially when material is treated at elevated temperatures. In this situation, the using of carefully prepared

 ©2005 The American Physical Society

TABLE I. Summary of material properties of granular samples.

Sample name	Average grain size (μm)	Purity (at. %)
N	~0.01	>99.9
SM	~0.4	>99.99
NE (acicular)	~0.7×0.1	99.6 (~0.3 % Ti)
M	~3	>99.9
L	30–60	>99.9

bulk polycrystal is helpful in elimination of side oxidation and in separation of the effects of nonstoichiometry.

The aim of this report is to present the results of our study of the effects of intergrain connectedness and oxidation on the MR in bulk magnetite. The conditions for MR observation have been revealed, and the experimental results have been explained within magnetically inhomogeneous GB model. The analysis of appropriate spin-selective scattering mechanisms indicates that the deviation from stoichiometry is a necessary condition for GB MR appearance.

The paper is organized as follows. Section II contains description of material properties, sample preparation procedures, and experimental methods. In Sec. III A, the conductivity of high-quality stoichiometric polycrystals of magnetite is described. The effect of GBs on conductivity and MR is analyzed. In Sec. III B, the MR and conductivity properties of granular samples of magnetite are presented. The effects of GB composition and point contact geometry on MR are analyzed in Sec. III B 1. Section III B 2 analyzes the general effect of oxidation on MR and conductivity of magnetite for granular topology of sample. In Sec. III C, the idea of inhomogeneous magnetic structure of GB is introduced and applied to GB MR model. This MR model is discussed in Sec. III D for the spin scattering in the limit of band or hopping conductivity. In Sec. III E, we consider an origin of low-field MR component and its connection to GB properties.

II. EXPERIMENTAL DETAILS

Bulk ceramics of magnetite were prepared through conventional sintering method from the 99.99% purity commercial magnetite powder. Temperature was varied in 1200–1350 °C range in order to control the grain size. Bulk density of polycrystalline samples was more than 95% (from x-ray density). Stoichiometric composition of samples was controlled during the sintering and cooling by adjusting of CO/CO_2 flow composition according to the diagram from Ref. 15. In order to remove the residual stress, the vacuum annealing was applied to the sintered samples for 60 h at 600 °C. Finally, samples of $12\times2\times1$ mm size were cut out from inner parts of larger ceramic blocks.

For the granular samples we have used a set of powders with various grain sizes, whose parameters are collected in Table I. The finest powder (*N*) with average grain size $d \approx 10\pm3$ nm was prepared by the coprecipitation method[16] from the mix of Fe^{2+} and Fe^{3+} ions in water solution by adding of ammonia. Then particles were washed by distilled water up to the neutral reaction of solution, separated by centrifuge, dehydrated in butanol, and finally dried at 75 °C under pumping (vacuum $\sim10^{-3}$ Torr) for 24 h. The rounded grain's shape and mean size *d* were revealed by transmission electron microscopy. The *d* value obtained was in agreement with one estimated from the broadening of x-ray powder diffraction peaks.

Particles *L* were prepared by the low-energy crashing of commercial granulated ceramic material in a mortar and subsequent separating by set of sieves. Each of these particles is composed by several smaller crystallites. Powder *M* was prepared by ball milling from the same raw material that was used for *L* powder. Also we have used a commercial powder of acicular particles (NE) with mean length about 700 nm and aspect ratio near 1:7, and the rounded shape particles (SM) of extra purity. All the powders were formed and finally palletized at a pressure 3 tons cm^{-2}. The precautions were made to minimize the exposure of the material to the air. Packing density of compacts lies in 50–65 % range.

In order to control of the granular sample's composition, we have used several annealing procedures. Because of the hardly avoidable surface oxidation and adsorption, the resistivity of as-prepared compact is badly repeatable and sensitive to the powder's preparation and storage history. We have applied a vacuum ($\sim10^{-2}$ Pa) annealing at 150 °C for 4 h to remove adsorbed species and normalize the surface/interface composition $Fe_{3(1-\delta)}O_4$ at some intermediate δ value. Also the flash annealing at 500 °C in $CO/CO_2=1/350$ gas mix flow for 30 min has been used to fix a throughout stoichiometric composition of the samples. The last procedure was verified to produce as highly stoichiometric composition as a standard reduction by H_2 in argon gas flow at 350 °C.[17]

In order to obtain a homogeneous sample's composition $Fe_{3(1-\delta)}O_4$ at the particular δ value, the annealing at 320 °C in closed CO/CO_2 atmosphere was applied for 30 h. For high δ, the annealing at 320 °C in N_2 flow for 30 h was also used. The latter procedure was found as more repeatable one. The special check for sample's homogeneity was made by using two different starting compositions of powders. We have used the pure magnetite and completely oxidized to maghemite γ-Fe_2O_3 compacts (of the same powder) for the simultaneous annealing. Both annealed samples have shown the identical composition, resistivity, and magnetic properties, which proves the stability of annealing procedure and homogeneity of the composition. All granular samples were finally shaped into $12\times2\times1.5$ mm parallelepiped.

X-ray powder diffraction and scanning electron microscopy were used to verify a single phase composition and to examine the sample's morphology. For chemical composition analysis, we have used a common titration technique[18] which allows us to determine δ value with 0.02% accuracy. Resistivity was measured using a standard four-probe method in the temperature range 50–350 K. Magnetic field was applied in perpendicular direction to the current in magnetoresistance measurements. Magnetization was measured using a vibrating sample magnetometer. The geometric demagnetization factors of samples were determined experi-

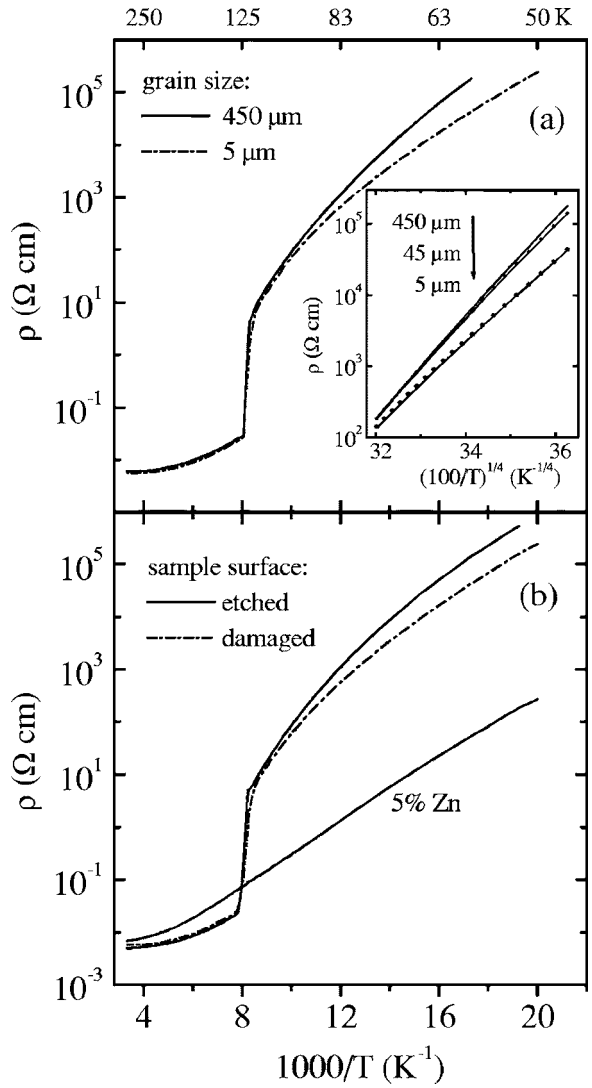

FIG. 1. (a) Resistivity of dense polycrystals with different grain sizes plotted as function of temperature $(1000/T)$. Inset: same resistivity data below T_V plotted as function of $(100/T^{1/4})$. For the samples with mean grain sizes of 5 and 45 μm, the experimental data are shown by points and the lines represent the results of fitting (for details see the text). For the sample with mean grain size of 450 μm, the experimental data are presented by a solid curve. (b) Resistivity of dense polycrystals with different surface quality and doped sample plotted as function of temperature $(1000/T)$.

mentally in the approximation of ellipsoid. Below we will use the H notation for the effective magnetic field H_{eff}.

III. RESULTS AND DISCUSSION

A. Dense polycrystals

The resistivity of dense stoichiometric polycrystals with average grain sizes of 5, 45, and 450 μm were measured. The corresponding temperature dependencies are shown in Fig. 1(a) and in the inset of Fig. 1(a). All samples display a Verwey transition characterized by 110–120 times jump in resistivity at 122–123 K, which reveals a high degree of stoichiometric composition.[19] At the temperatures above the Verwey transition temperature (T_V), the resistivity of polycrystals shows no dependence on the grain size. The absolute room temperature resistivity value is $5.5\pm0.5\times10^{-3}$ Ω cm, that is very close to the $4.5\pm0.5\times10^{-3}$ Ω cm reported for the stoichiometric monocrystal.[19,20] Thus, the resistivity data indicate that the GB partial resistance is negligibly small for these samples. This is consistent with the lack of MR effect within 0.05% detection limit.

In contrast, the resistivity below T_V displays a systematic dependence on grain size, as shown in the inset of Fig. 1(a), in such a way that the incorporation of GBs *decreases* the sample resistivity, which is opposite to the expected behavior. This dependence can be quantitatively expressed by Mott's variable range hopping (VRH) $(T_0/T)^{1/4}$ law, which is widely used for the approximation of magnetite resistivity below T_V.[20,21] The experimental data presented in the inset of Fig. 1(a) show that the resistivity could be reasonably linearized in $\ln(\rho)-(1/T)^{1/4}$ axis. The best fit (not shown in Fig. 1) gives $T_0=6.7$, 5.4 and 3.0×10^8 K values for grain sizes of 450, 45, and 5 μm, accordingly. These values could be compared to the $T_0=9.3\times10^8$ K, reported for 99.999% purity high quality monocrystal in Ref. 20.

Additionally, the resistivity below T_V was found to be sensitive to surface quality of sample. This is illustrated by Fig. 1(b) presenting the resistivity data for two samples with the same 45 μm average grain size and different surface condition. One sample was just as-prepared after diamond saw, and a second was chemically polished to remove about 20 μm of surface material layer. The presence of mechanically damaged surface layer results in lower sample resistivity with $T_0=3.5\times10^8$ K, as it is displayed in Fig. 1(b). We note that all other data presented in Fig. 1 was taken on chemically polished samples.

The observed sensitivity of low temperature resistivity to the grain size and surface quality could be directly explained from the nature of Verwey transition. It is known that the resistivity jump at Verwey transition is connected to the opening of band gap at the Fermi level after a long range charge ordering in conductive B sublattice.[22] Also it was known that the resistivity value below T_V is so sensitive to the sample stoichiometry, that the oxidation or doping at the $\sim$1 at. % level is followed by complete suppression of Verwey transition.[19] This effect is qualitatively common for the wide range of donor, acceptor, or isoelectronic types of dopant,[19,23] what indicates that it is driven by the random defect's potential and charge misbalance, rather than by the total carrier concentration. Thus, in the highly defective crystal lattice, which is supposed to characterize the GB and mechanically damaged surface layer, the charge ordering is expected to be destroyed by potential fluctuations from general stacking faults and local nonstoichiometry. In the absence of charge ordering, the finite density of states appears at Fermi level, providing a high conductivity. Further experimental support for that picture comes from the comparative studies of the photoemission spectra from the cleaved and scraped surface of magnetite reported in Ref. 24. Below T_V, the data from scraped surface demonstrated a metal-like density of states at the Fermi level, in contrast to a clear gap for the cleaved surface.[24]

From the above analysis, we propose that the GB and damaged surface layer have an increased conductivity below

T_V (for 2–3 orders of value as compared to the bulk) due to the locally suppressed charge ordering, and hence they can contribute essentially to total conductivity of polycrystal despite their small partial conductive cross section. For a quantitative verification of this picture, we fitted the conductivity of polycrystal below T_V within the phenomenological model of parallel conductivity by grain's bulk and GBs (surface layer) with conductive thickness of GB (surface layer) as a fitting parameter. For the model resistivity of GB, the data of the doped magnetite [see Fig. 1(b)] was taken, where the Verwey transition is suppressed by ~5 at. % Zn doping. This material represents well the typical resistivity range of the highly conductive doped (oxidized) magnetite.[25] For the bulk resistivity, the data from sample with 450 μm grain size was used. The results of the best fit are shown by solid lines in the inset of Fig. 1(a), and it gives 2.4 ± 0.2 nm value for the effective conduction thickness of GB. This value is comparable to the direct estimation of structural thickness of GB ($\approx$1 nm) in MnZn ferrites.[26] Similar fitting was applied to the resistivity of the sample with surface damaged layer, and the conductive thickness of surface layer of 2.5 ± 0.1 μm was obtained from the best fit. This value appears as a realistic estimation of the thickness of damaged surface layer after mechanical cut. Thus, the above estimations show that the conductivity of magnetite polycrystals below Verwey transition can be well explained by the enhanced partial conductivity of GBs (surface layer). This indicates the specific origin of any MR observed below the Verwey transition.

Based on mechanical stress accumulation, the alternative explanation of low-temperature resistivity might be considered. The stress could be caused only by the rhombohedral distortion at the Verwey transition, because the growth-related stress was released by post-annealing. The earlier studies of stress effect on conductivity showed that the low temperature resistivity and T_V value are decreasing simultaneously with a stress.[27] Thus, the essential macroscopic stress accumulation should be accompanied by T_V downshift, which is not observed in our experiment. Hence the stress effects can be ruled out.

B. Granular samples

1. GB modification

The lack of MR effect observed above Verwey transition might be related to the low partial GB resistance. In case of granular samples, the partial GB resistance can be increased by using the smallest grain size d, geometrical constriction of intergrain contacts, and GB oxidation.

In the limit of point contact for intergrain contact spot size r_c ($r_c \ll d$), the resistance of a single contact can be presented by composition of the GB resistance $\rho_g/(\pi r_c^2)$ and resistance of the grain's bulk on the depth L from the contact where the main part of contact potential drops. For the negligible GB resistance, the L is of the order of r_c, and the contact resistance, estimated in Maxwell limit,[28] is $R_C=\rho_{\text{bulk}}/(2r_c)$, where ρ_{bulk} is an intrinsic bulk conductivity of magnetite. Then the granular sample resistance ρ, estimated from the average single contact resistance, is

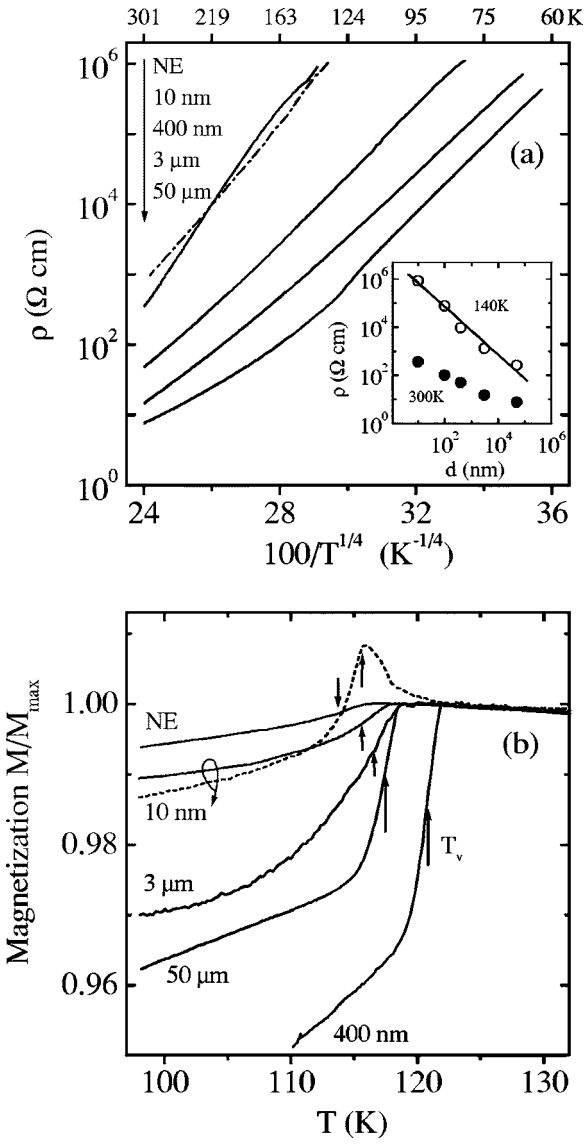

FIG. 2. (a) Resistivity of GB-oxidized granular samples with different grain sizes plotted as a function of temperature ($100/T^{1/4}$). Inset: the resistivity versus grain size at $T=300$ and 140 K. The values of NE sample ($d=100$ nm) are corrected for the aspect ratio (see Sec. III B 1). (b) Normalized magnetization of GB-oxidized granular samples plotted as function of temperature after zero-field cooling to 77 K. The magnetization was recorded at the external field 1 T (solid curves) and 25 mT (broken curve). Arrows indicate the Verwey transition temperature.

$$\rho = R_C d = \rho_{\text{bulk}} d/(2r_c) = \rho_{\text{bulk}} N, \tag{1}$$

where N is the grain diameter to contact diameter ratio. Supposing this ratio holds roughly for all the grain sizes,[29] the sample resistance basically has no dependence on the grain size. Only for the acicular particles (NE), we suppose that r_c reflects the smaller size (needle's diameter), whereas d, used for ρ estimation, is a needle's length. Hence, the resistivity of NE sample obtained from Eq. (1) is expected to be increased approximately by the aspect ratio $\approx$7, as compared to compacts from rounded particles for the same N. For the domi-

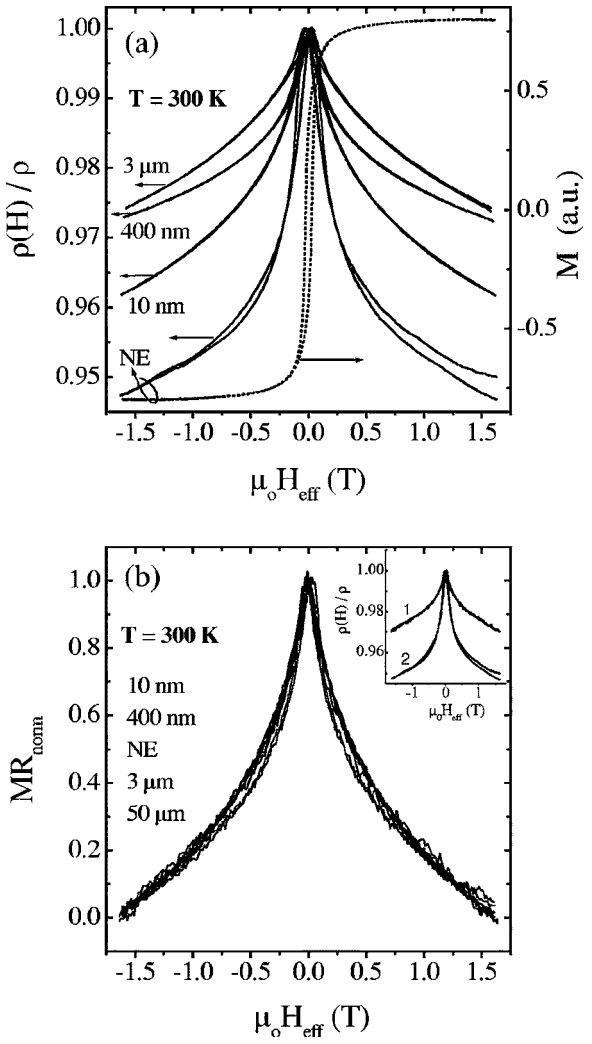

FIG. 3. (a) Solid lines are the magnetic field dependences of resistivity of GB-oxidized granular samples with different grain sizes at 300 K; broken line is the magnetization loop for NE GB-oxidized sample at 300 K. (b) Normalized magnetic field dependences of resistivity of stoichiometric granular samples with different grain sizes at 300 K. Inset: comparison of the magnetic field dependences of resistivity of NE samples with stoichiometric (1) and oxidized (2) GBs.

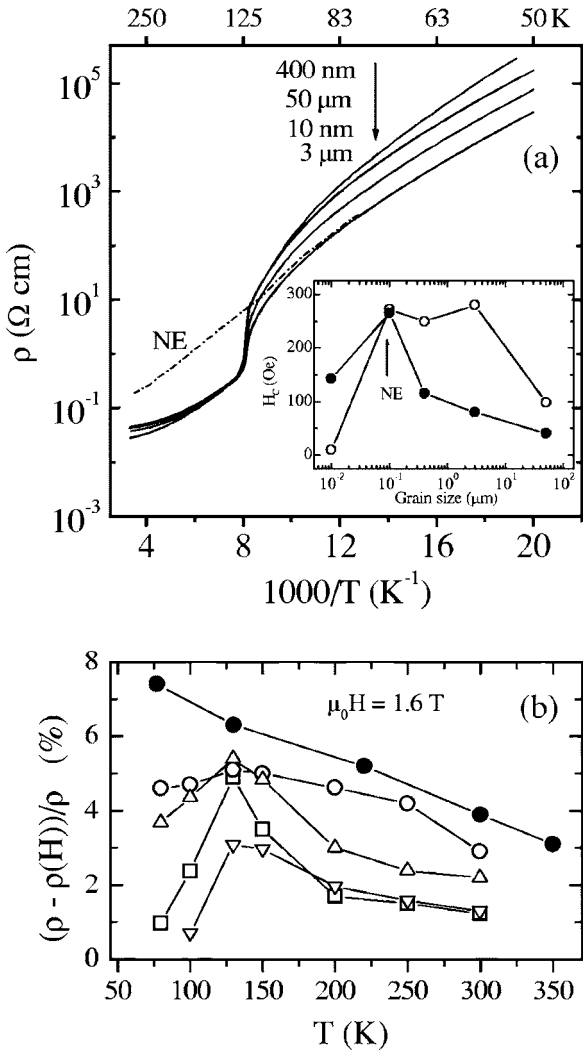

FIG. 4. (a) Resistivity of stoichiometric granular samples with different grain sizes plotted as function of temperature. Inset: coercive field values of granular samples plotted as function of grain size. Open symbols: GB oxidized, filled symbols: stoichiometric samples. (b) Magnetoresistance (UMR) as function of temperature. Open symbols: stoichiometric samples [squares: SM (400 nm), up triangles: N (10 nm), down triangles: L (50 μm), circles: NE]. Filled circles: homogeneously oxidized NE sample with δ=0.038.

nant GB resistance, the $L \ll r_c$ and the sample resistance is $\rho = R_C d = \rho_g N^2/(\pi d) \propto 1/d$—inversely proportional to the grain size.

First we consider the granular samples with surface composition $Fe_{3(1-\delta)}O_4$ normalized at some intermediate value δ by vacuum annealing at 150 °C. These samples mimic as-prepared compacts, but with well-repeatable properties. The temperature dependencies of resistivity for these samples are presented in Fig. 2(a). The resistivity displays a clear dependence on the grain size, which became close to $1/d$ dependence at lower temperatures, as expected for the dominant GB resistance [see the linear fit in the inset of Fig. 2(a) and note the normalizing correction for the NE sample]. The weak sign of the Verwey transition is detected only for the sample with largest grain size (L) [see Fig. 2(a)], which has a lowest partial GB resistance. This is consistent with an expected suppression of Verwey transition at the oxidized GBs. The bulk (grain's interior) Verwey transition was detected [Fig. 2(b)] from the jump in saturation magnetization. The magnetization (M) data were recorded at external field of 1 T after zero-field cooling. The T_V values were determined in the 114–122 K range from the inflection point of M-T curves. These T_V values indicate that the intragrain composition is close to the stoichiometric one.[19] Note that the lower T_V value of NE sample is connected to its impurity level[19] (see Table I). We should also note that T_V is not affected by external magnetic field,[30] which is demonstrated in Fig. 2(b) by extra M-T scan of sample N recorded at the field of 25 mT. In the latter case, the magnetization is not saturated. Hence, the peculiarity in M-T curve is supposed to be connected to the behavior of susceptibility near the phase transition, and T_V was determined from the maximum of

$M(T)$ in this case. In addition, from the fact that the Verwey transition is also observed for the smallest grain size ~10 nm (N), we can conclude that thickness of surface oxidized layer is limited by a few nm at most, i.e., it is close to the structural thickness of GB.

The above analysis indicates that GB resistance dominates the resistivity in GB-oxidized samples. Since the temperature dependences of resistivity are close to the $(T_0/T)^{1/4}$ law [Fig. 2(a)], the VRH might be considered as a mechanism of electron transport at GBs. But the limiting value of few nm obtained for GB-oxidized layer, is of the order of typical hopping length in VRH, which is hardly compatible with developed three-dimensional hopping inside GB. Then the combination of resonant tunneling via single localized state and sequential hopping via limited number of states seems to be a more appropriate model of electron transport across the oxidized GB. In the latter case, the expected temperature dependence of GB resistance[31] is not as strong as that observed in our experiment [Fig. 2(a)]. The possible additional contribution to the temperature variation of GB resistance will be discussed in Sec. III E. On the other hand, the investigation of current-voltage (I-V) curves at 80 K shows no deviation from the linear dependence up to ~5 mV per averaged intergrain contact. That might be connected to the low voltage range applied to the single contact, especially in a view of distribution of individual contact parameters in real sample.

MR was observed for all samples in this series. The typical room-temperature MR data are presented in Fig. 3(a). The MR value defined as $\mathrm{MR}=[\rho(0)-\rho(H)]/\rho(0)$ is at the range of at 2.5–5.5 % (at $\mu_0 H=1.6$ T), and it has no clear dependence on the grain size. MR for NE (acicular) sample exhibits the largest value that correlates with an observation in Ref. 7. All MR curves have a prominent high field component which appears well above the technical saturation of magnetization. This is demonstrated by magnetization $M(H)$ and magnetoresistance $\mathrm{MR}(H)$ curves for NE sample in Fig. 3(a). Such an unsaturated resistance indicates the magnetically hard behavior of GB. The MR value increases gradually in 1.5-2 times with decreasing temperature down to 80 K. Note that majority of MR characteristics, obtained from this series of samples, are consistent with the earlier report of MR properties of magnetite powder compacts.[7]

The next series of granular samples examined had a throughout stoichiometric composition fixed by flash annealing at 500 °C (see Sec. II). The Verwey transition was detected at ~122 K for most of the samples [see Fig. 4(a)], indicating a good stoichiometric composition.[19] The weak feature of the Verwey transition at ~115 K for NE sample well corresponds to its major contamination by Ti at 0.3% level.[19,32] The resistivity values are close for all grain sizes (spanned for four decades) at $T>T_V$, as shown in Fig. 4(a). According to Eq. (1), it indicates that GB resistance is very close to that for the equivalent layer of regular material, what correlates with the results for dense polycrystals discussed in Sec. III A. The increased resistivity of NE sample is consistent with the effect of particle shape (aspect ratio) discussed before. From the room-temperature resistivity values, the $N \approx 10$ was estimated, what testify the validity of the point contact approximation.

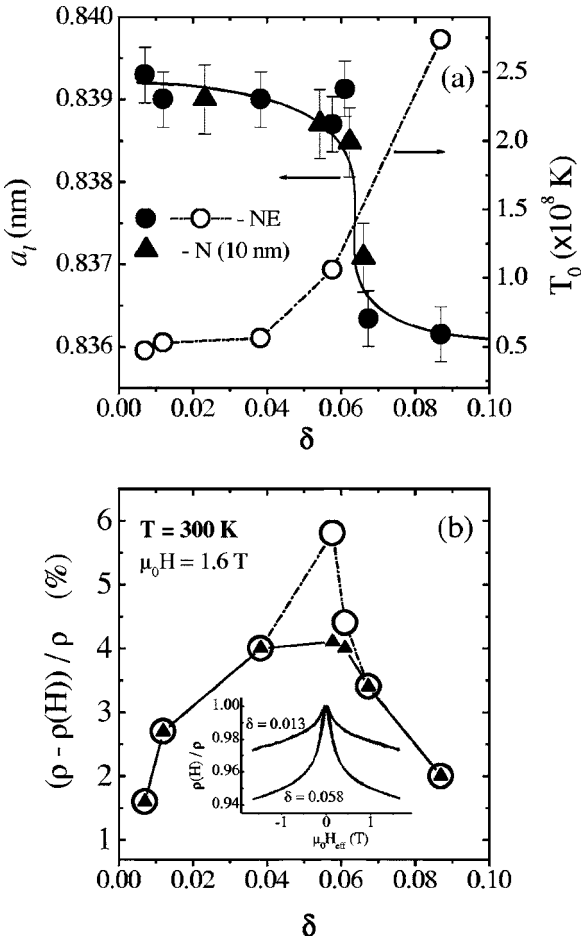

FIG. 5. (a) Crystal lattice parameter and T_0 as functions of oxidation (a solid line is merely the guide to the eye). (b) Magnetoresistance value as a function of oxidation at 300 K and $\mu_0 H = 1.6$ T. Open circles: total MR, filled triangles: UMR component. Inset: comparison of the magnetic field dependences of resistivity of NE samples with different oxidation values.

Surprisingly, considering the negligibly small GB resistance, the essential MR was observed for these stoichiometric samples. The room temperature MR value lies in 1.2–3 % range (at $\mu_0 H=1.6$ T) with larger values appeared for smaller grain sizes. The MR curves had an essential HF component similar to the data for GB oxidized case [compare Figs. 3(a) and 3(b)]. The main difference between two sets of MR data is an on average smaller LF MR component for the stoichiometric samples. This is more clearly observed for NE samples, as shown in the inset of Fig. 3(b). The most interesting result follows from the analysis of MR curves. As it is shown in Fig. 3(b), the normalized $\mathrm{MR}(H)$ curves for different grain size are very close, approaching the same "universal" shape. We will denote this shape the "universal" magnetoresistance (UMR). We suggest that this feature indicates the common MR mechanism which is not sensitive to the individual magnetic properties of grains. And in the following section we will present a model that is able to explain the phenomenon and reproduce this specific shape.

The MR value for all samples increases at 1.5–2 times after cooling down to 130 K without noticeable change in

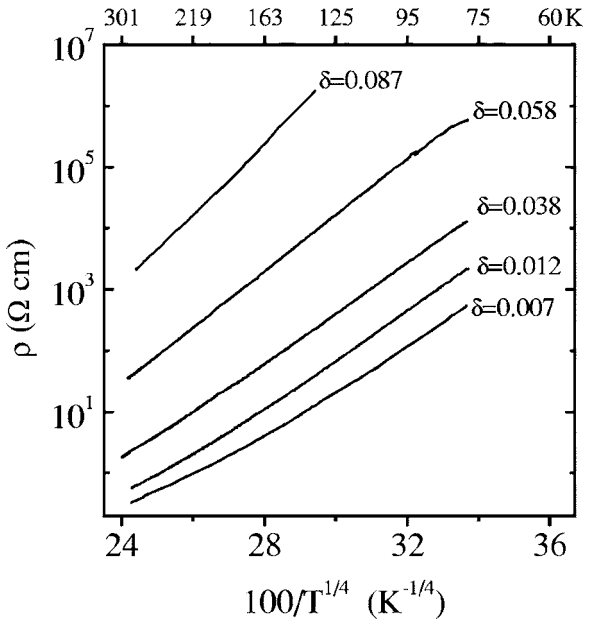

FIG. 6. Resistivity of homogeneously oxidized NE samples with different oxidation values plotted as function of temperature $(100/T^{1/4})$.

the MR(H) shape. At that, the MR of NE sample displays a steep growth just below 300 K with subsequent saturation, as shown in Fig. 4(b). For the rest of the samples, the MR displays an upturn at much lower temperatures. Note also the quenching of MR below T_V [see Fig. 4(b)], which is less prominent for NE than for the other samples.

Figure 4(a) shows the resistivity jump of 10–13 times at T_V, which is about one order less than expected for the stoichiometric magnetite (compare to Fig. 1). This difference cannot be explained from the impurity level. In addition, it is known from previous reports,[19] that the resistivity jump and T_V values are always decreasing simultaneously. In such a case, if all the material forming the point contact proceeds through Verwey transition, then the resistivity jump value should be as large as it corresponds to the T_V value. In agreement with results from dense polycrystals, we propose that the smaller jump value reflects the suppression of Verwey transition at GB and, possibly, at the surface of grains too. This explanation is strengthened by the low values of $T_0 = (1.6-1.9)\times 10^8$ K obtained from the $(T_0/T)^{1/4}$ fit below T_V. The resistivity for different grain sizes displays some scatter below T_V [see Fig. 4(a)]. In particular, the resistivity value is lower for the higher impurity level and smaller grain size, which is consistent with the expected effects from the incorporation of point defects and GBs.

The coercive field values H_c of stoichiometric granular samples drop essentially, as compared to the GB-oxidized case. The corresponding data are presented in the inset of Fig. 4(a). This difference indicates an enhancement of magnetic coupling across the GB due to the sintering. The increasing of H_c with sintering for N sample ($d \approx 10$ nm) could be due to the effect of building up the finite coercitivity after quenching a superparamagnetic state of grains by the interparticle interaction. Note also the stable H_c value for NE sample, which can be explained by strong shape anisotropy and small contact size to grain size (length) ratio.

We have checked the effect of further sintering on magnetic and transport properties of stoichiometric granular samples. The flash annealing at higher temperature (800 °C) in CO/CO_2 flow produces the qualitatively similar result to that at 500 °C. The absolute values of resistivity, MR and H_c drop further (as compared to the 500 °C annealing), displaying the progressive approach to the dense polycrystal's characteristics.

2. Compositional dependence

In order to separate the composition and sintering effects on MR and to obtain more detailed information about the role of stoichiometry, we have performed a series of measurements of samples with controlled oxidation. The granular samples NE and N types were homogenized at the oxygen composition $Fe_{3(1-\delta)}O_4$ intermediate between magnetite ($\delta=0$) and maghemite ($\delta=1/9$). The annealing applied (see Sec. II) has the same temperature and duration conditions for all δ, hence we can consider the sintering degree (N value) to be equal for all compositions. The only parameter changed is the oxidation degree δ. The bad sinterability of acicular grains (NE) helps to keep the point contact condition in granular sample after a long-time homogenizing annealing. In contrast, the N samples ($d \approx 10$ nm) display an essential sintering degree. Therefore we have used only the structural data from N samples.

The oxidation creates the iron-ion vacancies in octahedral B sites of the spinel lattice of magnetite and finally turns magnetite to the maghemite γ-Fe_2O_3 ($\delta=1/9$) which is a dielectric with band gap about[33] 2 eV. The structure of maghemite could be presented as a basic magnetite structure with ordered Fe vacancies in the B sublattice. Hence the structure of the intermediate composition $Fe_{3(1-\delta)}O_4$ is supposed to contain Fe-ion vacancies randomly placed in the B sublattice.

The lattice constant of oxidized samples is presented in Fig. 5(a) as a function of δ. The lattice parameter value was calculated from the x-ray K_{alfa1} peak position for (800) reflection of magnetite. Figure 5(a) shows a weak dependence of lattice parameter on oxidation at low δ, followed by a sharp drop near $\delta=0.058$, approaching the γ-Fe_2O_3 lattice parameter value (0.8352 nm). This dependence correlates with the variation of lattice parameter from oxidation in magnetite monocrystal reported in Ref. 34. We suggest that the abrupt change of lattice parameter indicates a transition to the γ phase.

The resistivity increases continuously with oxidation. The temperature dependences of resistivity for different compositions are presented in Fig. 6, and could be approximated by $(T_0/T)^{1/4}$ law, especially at low temperatures. The extracted T_0 parameter value [see Fig. 5(a)] changes quickly at $\delta \geqslant 0.058$, pointing to the increasing localization of electrons or replacement of key conductivity parameters. Note that analogous change in conductivity was observed[32] in monocrystals of doped magnetite $Fe_{3-y}Ti_yO_4$ at $y \approx 0.18$ that corresponds to the similar level of Fe-ion deficiency (for $3\delta \leftrightarrow y$ correspondence). Thus, the conductivity data are in qualita-

tive agreement with the suggested magnetite to γ-phase transition corresponding to metal-dielectric transition and occurred at $\approx 9\%$ deficit of the conducting B sites.

Room temperature MR values for oxidized samples are presented in Fig. 5(b). The MR value increases with the oxidation displaying a peak value at $\delta \approx 0.058$ and drops after the suggested transition to γ phase. Note that MR data for $\delta = 0.087$ are very close to that reported[35] for the compact of acicular particles of "slightly reduced" γ-Fe_2O_3. The MR value increases almost linearly up to 4.5–6.5% after cooling down to 130 K for $\delta < 0.058$ and up to $\sim 7.5\%$ for $\delta = 0.058$. A typical example of the MR temperature dependence is presented in Fig. 4(b) for $\delta = 0.038$. The MR curve shape is practically unaffected by temperature.

An analysis of MR shape shows that MR primary follows the "universal" MR (UMR) shape [Fig. 5(b)], with an additional LF component appeared only near $\delta \approx 0.058$. The MR data for $\delta \approx 0.058$ are almost identical in shape and absolute value to that of the GB-oxidized NE sample, as it appears from comparison of MR curves shown in the insets of Figs. 3(b) and 5(b). Also the temperature dependences of resistivity in both cases are following the $(T_0/T)^{1/4}$ law with comparable T_0 values [compare Figs. 2(a) and 6]. From such a similarity, we suggest that for the homogeneously oxidized sample at $\delta \approx 0.058$, the appearance of LF MR component is connected to isolating GB conditions, similar to the GB-oxidized samples. The isolating properties are more likely to originate from concentration of iron vacancies at GB and/or local transition to the γ-Fe_2O_3 phase. Also the disorder-induced metal to dielectric Mott transition at decreased electron concentration[36] could be discussed. The investigation of I-V curves for the $\delta = 0.058$ sample reveals a linear behavior up to ~ 1 mV per intergrain contact at 80 K. The above consideration indicates that the difference in MR properties between GB-oxidized and stoichiometric granular samples, that is a value of LF MR [see inset of Fig. 3(b)], is connected to the oxidation rather than to the sintering degree.

C. GB model

The presented experimental data show that MR could be observed, if the GB resistance is enhanced by oxidation or/and the point contact GB geometry is realized. Two components of GB MR can be separated. One is the UMR—it has a stable shape for the wide ranges of grain size, oxidation, and temperature. And this component is supposed to be different from the LF MR which is connected to the isolating GB only. Although the LF MR could be explained by tunneling across the homogeneous GB, the explanation of UMR needs some more specific model of GB transport.

Because of the essential high field component, the UMR is supposed to be related to hard magnetic defects. Already for that reason, the ordinary domain wall (even thinned because of the geometrical constriction) is not a satisfactory approximation of GB magnetic structure. From the other side, a model of completely disordered spins at GB also seems unacceptable in view of the very low GB resistance observed in stoichiometric samples. The complete spin disorder on the length of nearest-neighbor interatomic distances appears as highly resistive structure[37] for the 100% spin-polarized conductivity. In addition, the complete spin disorder within GB should result in an effective magnetic decoupling of contacting grains, whereas the experimentally observed rapid drop of the coercive force with sintering [see inset of Fig. 4(a)] points to the essential coupling across GB. The hypothetic coherent antiferromagnetic coupling at GB creates a strong spin variation at the distance comparable to the electron wave vector, and hence it will acts as a highly reflective barrier for the conducting band electrons. That should provide a strong effect on resistivity, as it appears in thin films of magnetite containing the extended antiferromagnetic defects at antiphase boundaries.[12] Hence the model of coherent antiferromagnetic barrier is also inconsistent with our experimental data.

We propose that a more realistic approach could be based on the GB model including mesoscopic magnetic inhomogeneities. The corresponding magnetic structure could be modeled by distribution of local highly resistive areas of spin disorder—magnetic defects, interpolated by more smooth spin variations. These interpolating areas are supposed to have a low resistance and provide the highly conductive property of GB. The magnetic defects (or group of defects) are associated with crystal lattice imperfections. The local high anisotropy from the strain fields at crystal defects, local antiferromagnetic coupling, and surface anisotropy near pores—basically any origins might be considered, which fix the magnetization firmly or create the antiferromagnetic ordering. In our case the more important type of magnetic defect is the antiferromagnetic (AFM) one, as it is stable at high external field. This type of magnetic defects can appear from the local modification of superexchange interactions by crystal defects. We note that the crystal defects could be specifically disturbing for ferrimagnetic structures similar to magnetite, as the delicate balance of two strong antiferromagnetic interactions (resulted in bulk ferrimagnetic ordering) could be easily destroyed, following in the local antiferromagnetic ordering.[38] Experimentally, the AFM defects in magnetite were directly observed at the antiphase boundaries[11] and general stacking faults[39] in thin films.

The key point of our model is a magnetic structure surrounding the hard magnetic defects. Because of the local character of magnetic perturbation by defect, the magnetization in the surrounding area gradually approaches bulk direction or direction resulting from a joint action of neighboring defects. The thickness λ of such a magnetization transition layer (TL) could be estimated similar to the width of Bloch domain wall: $\lambda \approx \pi\sqrt{A/K_{\text{eff}}}$, where A is the exchange stiffness constant and $K_{\text{eff}} = K + K_{\text{sh}} + K_{\text{stray}}$ is an effective anisotropy constant composed by crystal anisotropy K, grain shape anisotropy K_{sh}, and magnetostatic term K_{stray}. The last term is size-dependent parameter, which becomes essential (of order J^2/μ_0) when size of magnetic defect (or group of defects) is comparable to or smaller than a bulk domain wall's width. For soft magnetic like magnetite, the minimal λ value is limited by the exchange length[40] $\lambda_{\text{ex}} \approx \sqrt{2\mu_0 A/J^2}$, that is 9 nm for the saturation magnetic polarization $J = 0.6$ T[41] and $A = 1.1 \times 10^{-11}$ J/m of magnetite. Here the exchange stiffness constant value was estimated in two-sublattice approximation[42] as $A = (2J_{AA}S_A^2 + 4J_{BB}S_B^2$

$-11J_{AB}S_AS_B)/2a_l$, where exchange constant values $J_{AA}=-11$ K, $J_{BB}=3$ K, and $J_{AB}=-22$ K were taken from Ref. 43; $S_A=2.5$ and $S_B=2.25$ are averaged spin values for iron ions in A and B sublattices, respectively, and $a_l=0.839$ nm is lattice constant. Note that the exchange length value (≈ 9 nm) is much smaller than the bulk domain wall's width $\sim\pi\sqrt{A/K}\approx 200$ nm.

In our inhomogeneous GB model, we assume that the spin scattering is high for the magnetic (AFM) defects and it gradually drops within the transition layers to much lower values at the interdefect regions, where the spatial spin variation is slow. This assumption appears reasonable, as the spin scattering will depend sensitively on the degree of spatial spin variation for any spin scattering model. The specific scattering mechanisms will be discussed later. When the external magnetic field is applied then the AFM defects remains stable[11,44] and the TLs shrink. Hence the areas of the slowest magnetization variation effectively expand. That results in an increasing of effective spin-conductive GB cross section in expense of spin-scattering crossection value, and provides an origin for the negative ''universal'' MR component in GB. Resistance of dense polycrystals is not sensitive to the supposed variation of GB conductive cross section, as long as partial GB resistance is negligibly small. In contrast, the resistivity of granular samples depends sensitively [see Eq. (1)] on conductive area of intergrain point contact due to the geometrical constriction. And this is valid for any value of the specific GB resistance (equal to or larger than the bulk one).

If the spin-selective scattering in TLs is very high, then additional conditions must be formulated for the GB model to be consistent with low GB resistance. The interdefect conductive areas should have an extension size larger than their separation distances.[45] In other words, this condition means that the resistivity of each inhomogeneous GB still has to be described more as a single conductive area rather than as a set of independent point contacts.

In the following, we will determine the UMR expression from the inhomogeneous GB model. The variation of GB magnetic structure at external field starts from the shrinking of widest transition layers and then goes for thinner TLs, as the field value sequentially reaches levels corresponding to their effective anisotropy K_{eff}. The MR starts to work effectively, when external field affects more spin-resistive transition layers. The quantitative expression for UMR could be directly obtained in approximation of one effective TL with thickness λ_{eff}. Validity of this approximation depends on real dispersion of λ and sensitivity of TL's resistivity to the spatial spin variation, and it will be discussed later in connection to the possible spin scattering mechanisms. We approximate the conductive point contact size r_C as $\sqrt{S_{\text{eff}}}$. Here S_{eff} is an effective conductive cross section of point contact, defined as a weighted difference between geometrical contact area S and summary area S_{TL} of TLs within the contact: $\sigma S_{\text{eff}} \equiv \sigma(S-S_{\text{TL}})+\sigma_{\text{TL}}S_{\text{TL}}=\sigma[S-(1-\sigma_{\text{TL}}/\sigma)S_{\text{TL}}]$. Here σ and σ_{TL} are the conductivities of regular material and TL accordingly. We have neglected the cross section area of the AFM defects themselves. Because the defect's resistance is supposed to be high and field-independent (in field range of interest), the inclusion of their area into consideration would simply renormalize the S value. Then the UMR expression appears as

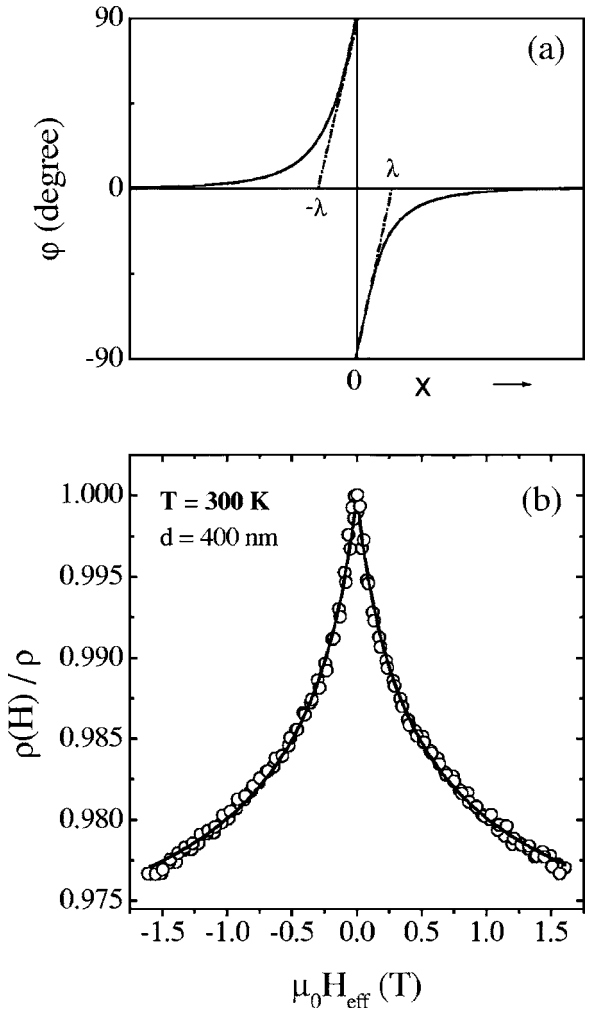

FIG. 7. (a) Schematic distribution of angle produced by local magnetization and external magnetic field in one-dimensional model of AFM defect. (b) Magnetic field dependence of resistivity (UMR) of stoichiometric SM sample at 300 K; symbols: experimental data, lines: fitting with Eq. (6).

$$\text{UMR}=\frac{R(H)}{R(0)}=\frac{r_C(0)}{r_C(H)}\approx\sqrt{\frac{S-(1-\sigma_{\text{TL}}/\sigma)S_{\text{TL}}(0)}{S-(1-\sigma_{\text{TL}}/\sigma)S_{\text{TL}}(H)}}$$
$$=\sqrt{\frac{S-(1-\sigma_{\text{TL}}/\sigma)P\lambda_{\text{eff}}(0)}{S-(1-\sigma_{\text{TL}}/\sigma)P\lambda_{\text{eff}}(H)}}, \quad (2)$$

where P is parameter which has a meaning of total perimeter length of the effective TL.

To obtain the field dependence of TL's thickness $\lambda(H)$, we will consider a one-dimensional model of AFM defect, following the consideration from Ref. 44. The stable state of the AFM defect[44] in external magnetic field larger than $\sim 0.02K_{\text{eff}}/J=0.01$ T is schematically presented in Fig. 7(a). (Below this critical field, the configuration rotates as a whole in respect to the field direction.[44]) There φ is an angle between local magnetization and external magnetic field. The φ_0 is still close to $\pi/2$ at the fields up to the exchange field

range.[44,11] Thus for the field range of interest, it is sufficient to consider the $\lambda(H)$ dependence in the configuration shown in Fig. 7(a). The energy density for the TL is

$$\gamma(H) = \int_{-\infty}^{0} \left[K_{\text{eff}} \sin^2 \varphi + HJ(1 - \cos \varphi) + A\left(\frac{d\varphi}{dx}\right)^2 \right] dx. \tag{3}$$

Following the variational calculus procedure, the integrated condition for minimum energy can be written as

$$K_{\text{eff}} \sin^2 \varphi_0 + HJ(1 - \cos \varphi_0) = A\left(\frac{d\varphi}{dx}\right)^2_{x=0}. \tag{4}$$

From this equation the width of TL in a linear approximation can be obtained, as it is shown by the trace line in Fig. 7(a):

$$\lambda(H) = \frac{\pi}{2}\sqrt{\frac{A}{K_{\text{eff}} + HJ}}. \tag{5}$$

Substituting Eq. (5) in Eq. (2), we have the field dependence of UMR in form

$$\text{UMR}(H) \approx \sqrt{\frac{1 - a/\sqrt{b}}{1 - a/\sqrt{b + H}}}, \tag{6}$$

where $a = \lfloor \frac{1}{2}(1 - \sigma_{\text{TL}}/\sigma) P\pi\sqrt{A/J} \rfloor / S$ and $b = K_{\text{eff}}/J$ are free parameters. Equation (6) was used to fit the experimental "universal" MR curve, and it reproduces the experimental data quite well for the approximation by one effective $\lambda_{\text{eff}}(H)$, as is illustrated in Fig. 7(b) for the stoichiometric SM sample. The best fits for other stoichiometric and homogeneously oxidized granular samples (except $\delta = 0.058$) give the $\mu_0 b$ parameter values in the 0.30–0.55 T range, which corresponds [see Eq. (5)] to the strong magnetostatic term K_{stray} and $\lambda_{\text{eff}} = 10-12$ nm $\approx \lambda_{\text{ex}}$. Also from the same fits the $a/\sqrt{b} = (1 - \sigma_{\text{TL}}/\sigma)(P\lambda_{\text{eff}})/S$ values at 0.05–0.1 and 0.05–0.15 ranges were obtained for stoichiometric and oxidized samples accordingly. From these parameters, the limit for $\sigma_{\text{TL}}/\sigma$ can be obtained, where Eq. (6) has a physical meaning. From the definition $(P\lambda_{\text{eff}})/S \equiv S_{\text{TL}}/S < 1$, hence we have $\sigma_{\text{TL}}/\sigma < (1 - a/\sqrt{b}) = 0.85$.

We would like to note that our model of inhomogeneous GB, when extended to the limit of high density of AFM defects, can provide an interpolating connection to the case of completely disordered GB. When the magnetic defect's separation distances become smaller than the exchange length, the resulted magnetic structure of GB is supposed to be "dead" (except the rotation as a whole part) at the external field lower than some H_{cr}. This H_{cr} is determined by the average defect separation $\Delta l = \lambda_{\text{eff}}$ value from Eq. (5), and can be written in the form $H_{\text{cr}} = A/\lfloor J(\pi/2\Delta l)^2 \rfloor$. When the external field reaches the H_{cr} range, the individual transition layers will be formed around defects and then shrunken with the field. That provides the UMR component [Eq. (6)] with $K_{\text{eff}} = JH_{\text{cr}}$. This approach shows that magnetically inhomogeneous GB model produces unavoidable "spin leaks" at external magnetic field. Also, we believe this model might be effective in explanation of resistivity and MR in other highly defective magnetite structures, such as ultrathin films.[11]

We would like to note that in our MR model the external field modifies the scattering area of TLs but not the conductivity of magnetic defects itself via paraprocess, in contrast to the other MR models for magnetite.[12] At the same time, the approach used is in resemblance to the magnetotransport modeling in frustrated metallic ferromagnets.[46]

D. Scattering mechanisms

In this section, we analyze the possible microscopic spin scattering mechanism to justify the proposed UMR model. Before applying any model to our data, it is worth to summarize briefly the main features of conductivity of magnetite. According to Ihle and Lorenz's theory,[47] the conductivity of stoichiometric magnetite results from a superposition of polaronic band and hopping conduction channels with the band conductivity dominated at $T \leqslant 300$ K. The positive temperature coefficient of resistivity is connected to the temperature-dependent density of states at the Fermi level, originated from the short-range electron correlations.[47] The depleted density of states at the Fermi level is consistent with a number of experimental results (see examples in Refs. 24, 48, and 49). In particular, the room temperature carrier concentration was estimated within Drude model from optical conductivity data.[49] It was only 2–5 % from what was expected for the Fe^{2+} concentration.

We neglected any variation of GB magnetic structure with temperature in further considerations. This assumption is based on the weak ($\sim 5\%$) temperature variation[42] of saturation magnetization and exchange constants of magnetite below 300 K, which might be expected for the magnetic with high Curie temperature. The anisotropy field is also supposed to be temperature independent, as $K_{\text{eff}} \infty J$ in our case. In addition, the experiment revealed[50] that exchange interaction is not affected by Verwey transition as well.

1. Band conductivity

The MR sensitivity to oxidation points to the possible role of point defects (iron-ion vacancies) in spin scattering. The spin-selective defect scattering mechanism responsible for the additional resistivity of domain wall was proposed in Ref. 51 for ferromagnetic metals within two-channel model. This mechanism is generally based on defect scattering between the admixing states of opposite spin at Fermi level within domain wall. That is following in positive extra spin resistance of domain wall proportional to the squared value of spatial spin variation. We propose that the spin scattering of similar origin in TLs is responsible for the observed UMR in magnetite at low δ. The main difference from the original model is the supposed 100% minority spin polarization at the Fermi level of magnetite. The theoretical consideration of half metals predicts an existence of nonquasiparticle states near the Fermi level for majority spins in magnetite.[52] These states do not contribute essentially to the conductivity, although there is expected a probability for the scattering into these states mediated by defect's potential.[52]

The effective spin scattering requires that spin precession of traveling electron should be not very fast compared to the magnetization variation within TL, and it is epitomized in

Ref. 51 by parameter $\xi = h^2 k_F/(16\pi m \lambda J_{ex})$. Here k_F is the Fermi wave vector, m is the effective mass, and J_{ex} is the exchange splitting energy. The spin resistance, averaged for the current flow parallel and perpendicular to TL, can be written[51] in two-channel approximation ($\rho^{\uparrow}/\rho^{\downarrow} \gg 1$) as

$$\frac{\rho^D_{TL} - \rho^D}{\rho^D} = \frac{2\xi^2}{5}\frac{(\rho^{\uparrow} - \rho^{\downarrow})^2}{\rho^{\uparrow}\rho^{\downarrow}} \approx \frac{2\xi^2}{5}\frac{\rho^{\uparrow}}{\rho^{\downarrow}}, \tag{7}$$

where $\rho^D{}_{TL}$ and ρ^D ($1/\rho^D = 1/\rho^{\uparrow} + 1/\rho^{\downarrow}$) are the defect scattering terms of material resistance with and without TL accordingly. For the nominally stoichiometric samples, the spin resistance of TL is supposed to originate from the scattering by potential fluctuation introduced by interface disorder and residual point defects. For the quantitative estimation we choose values $\lambda = 9$ nm, $m/m_e = 3$, $E_F = 0.5$ eV,[3] and $J_{ex} = 2$ eV.[3] With these parameters and $\rho^{\uparrow}/\rho^{\downarrow} \geq 10^4$, the $(\rho^D{}_{TL} - \rho^D)/\rho^D \geq 50\%$ was obtained. This estimation of spin-selective resistance of TL is consistent with the limit obtained from the fit of experimental data by Eq. (6). The absolute spin resistance value appears as not very high, which indicates that MR originates from the most resistive TL, such that it has a minimal thickness $\lambda \approx \lambda_{ex}$. That provides some ground for the approximation of single effective TL, used in derivation of Eq. (6).

According to the above spin-scattering model, the MR variation with oxidation, observed for low δ (≤ 0.01) values at 300 K [see Fig. 5(b)], corresponds to the variation of partial value of defect scattering term in total resistivity. This explanation could be verified by quantitative estimation of mean relaxation time for defect scattering from $\tau \approx (N_D \nu_F Q_{eff})^{-1}$, where the scattering cross section is defined as $Q_{eff} = \pi r_{TF}^2 = \pi \varepsilon_0/[e^2 N(E_F)]$, r_{TF} is the Thomas-Fermi screening length, ε_0 is the permittivity of vacuum, $\nu_F = \sqrt{2E_F/m}$ is the Fermi velocity, and $N_D = \delta N_0$ ($N_0 = 8 \times 10^{28}$ m^{-3}) is the defect concentration. By using the depleted density of states at Fermi level $N(E_F) = 0.1n/E_F$ [where $n = 2.7 \times 10^{28}$ m^{-3} is Fe^{2+} (electron) concentration] and realistic material parameters listed above, the $\tau = 1 \times 10^{-13}$ s is obtained for $\delta = 0.001$. This value is comparable to the mean relaxation time $(0.8-1.5) \times 10^{-13}$ s obtained from the application[47,53] of Ihle and Lorenz's conductivity model to experimental data at 300 K. Thus, this estimation shows that the defect scattering term becomes comparable to the scattering by phonons at $\delta \sim 0.001$ at 300 K. At higher δ the defect scattering dominates the resistivity, providing the saturation of MR value, which is in qualitative agreement with the data shown in Fig. 5(b).

Similar consideration could be applied to the temperature variation of MR. The temperature-dependent electron scattering is expected to be suppressed at lower temperature, providing the increasing partial value of the defect scattering term. Moreover, the defect scattering itself is expected to be more effective at low temperatures. This appears because of the further depleting of the density of states at E_F under cooling, following in increasing of the screening length r_{TF} and so the scattering cross section Q_{eff}. The resulted variation of the defect scattering term is supposed to provide the temperature dependence of MR. Hence, the temperature variation of MR is expected to be sensitive to the concentration of defects, which is consistent with experimental data shown in Fig. 4(b). The MR of NE sample (purity 99.6%) increases with cooling just from the room temperature [Fig. 4(b)], which is expected from the above estimation of defect scattering term for the $\sim 0.1\%$ doping level. The MR of other samples displays the upturn at much lower temperatures [Fig. 4(b)], which is in agreement with their higher purity ($>99.9-99.99\%$). In both cases the MR is expected to be saturated at the some value at low temperature, where defect scattering dominates the conductivity. According to the room temperature data shown in Fig. 5(b), this saturation MR value is $\approx 4\%$ for NE samples. The low temperature MR saturation of NE sample appeared at $\approx 5\%$ [Fig. 4(b)] which is close to the expected value. The small deviation might originate from some unaccounted weak temperature dependence or from variation of GB magnetic structure between different annealing procedures. For the more pure samples, the MR saturation is expected at lower temperature, but it is not observed because of the Verwey transition.

The quenching of MR below T_V [see Fig. 4(b)] is not related to the variation of scattering efficiency, but it simply follows from the supposed local suppression of Verwey transition at GB. In such a case, any contribution from GB to the resistance of intergrain contact is diminished below T_V. Since the resistivity jump value at T_V drops with defect concentration, the less effective quenching of MR is expected for the more defective samples (NE). And there is no quenching expected, when the bulk Verwey transition is totally suppressed (at $\delta > 0.01$), which is consistent with the experimental observations for higher δ [see Fig. 4(b)].

The band conductivity in magnetite is expected to be replaced or overwhelmed by hopping at some δ or at low temperature. Then the above proposed scattering mechanism is not applicable anymore and a hopping conductivity model should be considered.

2. Hopping conductivity

We will consider the modification of hopping activation energy arising from the spin variation within the transition layer. The interaction between hopping electron spin and Fe^{3+} ion magnetic moment can be expressed as a Hund's on-site exchange coupling energy $J_H \boldsymbol{s} \cdot \boldsymbol{S}$, where $\boldsymbol{s}$ and $\boldsymbol{S}$ are normalized moments of conduction electron and Fe^{3+} ion accordingly. In case of electron travel across TL, the angle φ between the spins of Fe ions, where electron is hopping, is not zero and contribution to the activation energy arises due to the magnetic interaction $E_M = J_H(1 - \cos\varphi)$. We can write φ as $\pi l_h/2\lambda$, where l_h is the hopping length. For quantitative estimation of the impact of this magnetic interaction on total resistivity of TL, we need the realistic hopping parameters.

The resistivity of oxidized sample at $\delta = 0.038$ follows close to $(T_0/T)^{1/4}$ dependence with $T_0 \approx 0.5 \times 10^8$ K for all registered temperature range, as it is shown in Fig. 6. Supposing the VRH characterizes the conductivity in this sample, the E_M value can be estimated from the evaluation of the hopping length.[36] The localization parameter could be obtained[36] as $\alpha^{-1} = [kT_0 N(E_F)/16]^{-1/3} = 0.06$ nm, and the average hopping length[36] is $l_h = \frac{3}{4}\left[\frac{2}{3}\pi\alpha N(E_F) kT\right]^{-1/4} = 0.94$ nm

at 300 K. Then $E_M = J_H[1-\cos(\pi l_h/2\lambda)]$ is 17 meV for $\lambda = 11$ nm (obtained from the UMR curve fit) and $J_H \approx J_{ex} = 2$ eV from Ref. 3. This E_M value is much lower than the activation hopping energy $E_A = \left[\frac{4}{3}\pi l_h^3 N(E_F)\right]^{-1} = 120$ meV, hence we can assume that the incorporation of magnetic interaction (E_M) will not affect the hopping length essentially. Then the resistivity of TL can be written as $\rho_{TL} \approx \rho_0 \exp[2\alpha l_h + (E_A + E_M)/kT]$. From here the spin-sensitive resistivity of TL is

$$\rho_{TL}/\rho \approx \exp(E_M/kT). \tag{8}$$

That gives $\rho_{TL}/\rho \approx 2$ at 300 K, which is consistent with applicability range of Eq. (6). Also, the strong exponential dependence of spin resistance on λ justifies the application of single effective TL thickness [λ_{eff} used in derivation of Eq. (6)] as a steepest descent approximation.

Next we consider temperature dependence of MR. The Eq. (8) was obtained for $E_M \ll E_A$ approximation which is no longer true at low temperatures, as the l_h (and so E_M) is increasing and E_A is decreasing under cooling. However, we can estimate the scale of temperature variation of MR by using the facts that MR still follows the UMR shape at low T and that Eq. (6) is saturating quickly at $\rho_{TL}/\rho \gg 1$. The last condition is satisfied for $T \sim 50$ K for $E_M \geq 17$ meV. Then the low-temperature MR limit could be estimated from Eq. (6) by using a and b values obtained from the UMR curve fit at 300 K. For that we consider the temperature dependence of a:

$$a(T) = a(300\text{ K})\frac{[1-\sigma_{TL}(T)/\sigma(T)]}{[1-\sigma_{TL}(300\text{ K})/\sigma(300\text{ K})]}$$

which approach the

$$\sim a(300\text{ K})/[1-\sigma_{TL}(300\text{ K})/\sigma(300\text{ K})]$$

value at low temperatures $[\sigma_{TL}(T)/\sigma(T) \ll 1]$. Substituting this expression in Eq. (6) and using the room-temperature values of $a/\sqrt{b} = 0.137$, $\mu_0 b = 0.48$ T, and $\sigma/\sigma_{TL} = \rho_{TL}/\rho \approx 2$ for NE sample with $\delta = 0.038$, the low-temperature saturation value of MR $\approx 8\%$ was obtained for $\mu_0 H = 1.6$ T. This value is consistent with the experimental temperature dependence of MR presented in Fig. 4(b).

E. Low field MR component

We have connected the appearance of LF MR component for homogeneously oxidized sample with $\delta \approx 0.058$ and for GB-oxidized granular samples to the conductivity across the isolating GB. Although the oxidation definitely enhances the GB resistance, the interpretation of isolating properties within tunneling model is not straightforward. That follows from the strongly activated temperature dependence of resistivity, presented in Figs. 2(a) and 6, which is hardly compatible with simple tunneling and might reflect a temperature-dependent parameter of the tunneling barrier. In the following, we will consider one of the possible explanations. The supposed GB barrier is characterized by the gamma-phase layer and the adjacent charge-depleted layers which appear due to the difference in work function between GB and bulk.[54] The depletion layers will affect the density of interface states which involved into tunneling. In addition if the charge depletion is strong enough to produce a band bending above the Fermi level, then the tunneling barrier expands into the depletion layers. The oxidized GB thickness was estimated at 1–2 nm, and the depletion layer decays at a distance of the order of $r_{TF} \approx 0.2$ nm. Hence, the depletion layers could be an essential part of the tunneling barrier. The temperature variation of charge density and its distribution within depletion layers is expected from the temperature dependence of density of conducting states in magnetite.[47] Thus, the observed temperature dependence of GB tunneling could be explained by temperature variation of the barrier width and interface density of states, which appear due to the strong electronic correlations in magnetite. If we turn to the MR, the multistep tunneling will contribute a little into MR, as the spin information is expected to decay quickly in a sequential process.[55] In this situation, the major part of MR is expected from the low order tunneling which can dominate at some links. We will consider the second order tunneling, following the model proposed in Ref. [56]. Supposing the uncorrelated magnetization in neighboring grains and negligible average GB magnetization at zero field, the field-dependent GB resistance $R(H)$ can be approximated[56] at the magnetic field just above the bulk saturation as

$$\begin{aligned} R(0)/R(H) &\propto 1 + 2\boldsymbol{M}\cdot\langle\hat{s}_{GB}\rangle + \langle(\boldsymbol{M}\cdot\hat{s}_{GB})^2\rangle \\ &= 1 + 2\boldsymbol{M}\cdot\langle\hat{s}_{GB}\rangle + 1/3M^2. \end{aligned} \tag{9}$$

Here the $\boldsymbol{M}$ and $\langle\hat{s}_{GB}\rangle$ are normalized values of bulk and GB magnetization accordingly. The third term corresponds to the LF MR component, which supposed[56] to reach the maximum value of 25%. The much lower experimental values of LF MR [Figs. 3(a) and 5(b)] might reflect the essential contribution from the higher order tunneling into GB conductivity. Another reason is the magnetic coupling of the interface states at both sides of GB, which might be essential because it is characterized by spin correlation on the distance of the order of exchange length which exceeds the isolating GB thickness. We believe this coupling is responsible for the observed difference in LF value between the samples [see Fig. 3(a)], as it is sensitive to the magnetic properties of the grains. In particular, the strongest LF component appears for NE sample because of the weakest effective magnetic coupling in this sample due to the largest shape anisotropy and lowest contact-size to grain-size ratio.

The second term in the right part of Eq. (9) contains a field-induced magnetization of grain boundary states. The GB magnetization in our model develops by contracting of transition layers [Eq. (5)] rather than by paramagnetic response of magnetically hard defects. Hence the $\langle\hat{s}_{GB}\rangle$ is expected to follow the "law of the approach to saturation" with the main component proportional[57] to $(1-\text{const}/H^{1/2})$. The field dependence of $\langle\hat{s}_{GB}\rangle$ could be obtained in terms of one effective λ_{eff}, which in this case characterizes the TL with the largest area within GB. Supposing the width of GB tunneling barrier is smaller than λ_{eff}, we obtain $\langle\hat{s}_{GB}\rangle \propto [1 - P\lambda_{eff}(H)/S]$, where P and S have the same meanings as

those used in Eq. (2). By using this estimation of $\langle \hat{s}_{GB} \rangle$ and Eq. (5), Eq. (9) can be transformed to

$$R(H)/R(0) \propto \left(1 - \frac{\text{const}}{\sqrt{K_{\text{eff}}/J + H}}\right)^{-1}, \qquad (10)$$

which is the analog of the squared form of Eq. (6). Due to the slow character of square root function, Eq. (10) mimics the UMR shape of Eq. (6) and, in general sense, simply reproduces the basic field dependence of spin-sensitive conductive cross section of GB planted in GB model. Finally, the combination of LF and UMR-like components of MR obtained from Eq. (9), appears in qualitative agreement with the experimental data in Figs. 3(a) and in the inset of Fig. 5(b).

The optimization of LF MR is especially important from the point of its potential in applications. From the analysis of our results, we propose that an effective approach to realization of magnetite-based spin-valve structures must eliminate the appearance of AFM defects. For example, it could be realized by trapping the thin domain wall in geometrical constriction[58] which is not superimposed with GB.

IV. CONCLUSIONS

In conclusion, we have shown that the structural disorder within GB is followed by specific magnetotransport properties of magnetite. The extra resistance, originated from carrier scattering at GBs, was found to be negligibly small in the stoichiometric magnetite. Moreover, the structural disorder and local nonstoichiometry within GB are supposed to be responsible for the local suppression of long-range charge ordering below Verwey transition, resulting in strongly enhanced in-GB conductivity. The low value of GB resistance is consistent with the lack of MR effect in dense stoichiometric polycrystals. At the same time, it was shown that MR response from the natural GB can be revealed by using GBs in the point contact limit. For the latter case, the magnetically and structurally inhomogeneous GB model was proposed to explain the coexistence of negligible GB resistance and MR response. The spin-dependent scattering in transition layers of magnetization surrounding the magnetic defects in GB was proposed as a basic origin for the observed MR. The model is able to reproduce the major characteristic of the experimental MR data. The microscopic mechanisms of spin scattering were analyzed, and MR variation with oxidation and temperature was discussed. The microscopic analysis indicates the important role of point defects in magnetotransport of magnetite.

The additional low-field component of GB MR was separated at high GB oxidation in granular samples of magnetite and associated with tunneling across the isolating GB. The low value of LF MR is assigned to the poor isolating performance of the oxidized GB and magnetic coupling of grains.

ACKNOWLEDGMENTS

This work was supported in part by the Japan Science and Technology Corporation.

[1] A. Gupta and J. Z. Sun, J. Magn. Magn. Mater. **200**, 24 (1999); P. M. Levy and S. Zhang, Curr. Opin. Solid State Mater. Sci. **4**, 223 (1999); M. Ziese, Rep. Prog. Phys. **65**, 143 (2002).

[2] A. Yanase and K. Siratory, J. Phys. Soc. Jpn. **53**, 312 (1984).

[3] Z. Zhang and S. Satpathy, Phys. Rev. B **44**, 13319 (1991); R. A. de Groot and K. H. J. Buschow, J. Magn. Magn. Mater. **54–57**, 1377 (1986).

[4] Yu. S. Dedkov, U. Rüdiger, and G. Güntherodt, Phys. Rev. B **65**, 064417-1 (2002).

[5] V. V. Gridin, G. R. Hearne, and J. M. Honig, Phys. Rev. B **53**, 15518 (1996).

[6] X. W. Li, A. Gupta, G. Xiao, and G. Q. Gong, J. Appl. Phys. **83**, 7049 (1998); M. Ziese, R. Hohne, H. C. Semmelhack, H. Rechentin, N. H. Hong, and P. Esquinazi, Eur. Phys. J. B **28**, 415 (2002).

[7] J. M. D. Coey, A. E. Berkowitz, L. Balcells, F. F. Putris, and F. T. Parker, Appl. Phys. Lett. **72**, 734 (1998).

[8] J. J. Versluijs and J. M. D. Coey, J. Magn. Magn. Mater. **226–230**, 688 (2001); J. J. Versluijs, M. A. Bari, and J. M. D. Coey, Phys. Rev. Lett. **87**, 26601 (2001).

[9] P. Seneor, A. Fert, J.-L. Maurice, F. Montaigne, F. Petroff, and A. Vaures, Appl. Phys. Lett. **74**, 4017 (1999).

[10] X. W. Li, A. Gupta, G. Xiao, and V. P. Dravid, Appl. Phys. Lett. **73**, 3282 (1998); P. J. van der Zaag, P. J. H. Bloemen, J. M. Gaines, R. M. Wolf, P. A. A. van der Heijden, R. J. M. van de Veerdonk, and W. J. M. de Jonge, J. Magn. Magn. Mater. **211**, 301 (2000); C. Srinitiwarawong and G. A. Gehring, J. Phys.: Condens. Matter **13**, 7987 (2001).

[11] D. T. Margulies, F. T. Parker, M. L. Rudee, F. E. Spada, J. N. Chartman, P. R. Aitchison, and A. E. Berkowitz, Phys. Rev. Lett. **79**, 5162 (1997); S. Celotto, W. Eerenstein, and T. Himba, Eur. Phys. J. B **36**, 271 (2003).

[12] M. Ziese and H. J. Blythe, J. Phys.: Condens. Matter **12**, 13 (2000); W. Eerenstein, T. T. M. Palstra, S. S. Saxena, and T. Hibma, Phys. Rev. Lett. **88**, 247204 (2002).

[13] L. Wang, J. Li, W. Ding, T. Zhou, B. Liu, W. Zhong, J. Wu, and Y. Du, J. Magn. Magn. Mater. **207**, 111 (1999); J.-M. Li, A. C. H. Huan, L. Wang, Y.-W. Du, and D. Feng, Phys. Rev. B **61**, 6876 (2000); C. T. Lie, P. C. Kuo, Wei-Chih Hsu, I. J. Chang, and J. W. Chen, J. Magn. Magn. Mater. **239**, 160 (2002).

[14] C. Zhang, S. Li, L. Wang, T. Wu, and S. Peng, Mater. Chem. Phys. **62**, 44 (2000).

[15] R. Dieckermann, Ber. Bunsenges. Phys. Chem. **86**, 112 (1982) and references therein.

[16] R. Massart, IEEE Trans. Magn. **17**, 1247 (1981).

[17] A. R. Corradi, IEEE Trans. Magn. **14**, 655 (1978).

[18] J. Brynestad and H. Flood, Z. Elektrochem. **62**, 953 (1958).

[19] Z. Kakol, J. Sabol, J. Stickler, and J. M. Honig, Phys. Rev. B **46**, 1975 (1992); R. Aragon, R. J. Rasmussen, J. P. Shepherd, J. W. Koenitzer, and J. M. Honig, J. Magn. Magn. Mater. **54–57**,

1335 (1986).
[20] N. Lenge, H. Kronmüller, and F. Walz, J. Phys. Soc. Jpn. **53**, 1406 (1984).
[21] S. B. Ogale, K. Ghosh, R. P. Sharma, R. L. Greene, R. Ramesh, and T. Venkatesan, Phys. Rev. B **57**, 7823 (1998).
[22] E. J. W. Verwey, Nature (London) **144**, 327 (1939).
[23] V. A. M. Brabers, F. Walz, and H. Kronmüller, Phys. Rev. B **58**, 14163 (1998).
[24] A. Chainani, T. Yokoya, T. Morimoto, T. Takahashi, and S. Todo, J. Electron Spectrosc. Relat. Phenom. **78**, 99 (1996).
[25] P. Wang, Z. Kakol, M. Wittenauer, and J. M. Honig, Phys. Rev. B **42**, 4553 (1990).
[26] P. J. van der Zaag, J. J. M. Ruigrok, A. Noordermeer, M. H. W. M. van Delden, P. T. Por, M. Th. Rekveldt, D. M. Donnet, and J. N. Chapman, J. Appl. Phys. **74**, 4085 (1993).
[27] M. Matsui, S. Todo, and S. Chikazumi, J. Phys. Soc. Jpn. **42**, 1517 (1977).
[28] N. Agrait, A. L. Yeyati, and J. M. van Ruitenbeek, Phys. Rep. **377**, 81 (2003).
[29] The ground for this equality follows from the same external pressure applied to compact the granular body for different grain sizes and scaling invariance of mechanical properties of grains. Here we suppose that for weak sintering conditions the intergrain contact size is determined by contact plastic deformation during the compacting process. We approximate the granular body as regular arrays of particles arranged in a simple cubic lattice. The contact size r_c is connected to the average pressure at the intergrain contacts at the end of deformation process through the static condition within array as $P_{\text{ext}}(\pi d^2/4) \approx P_{\text{contact}}(\pi r_c^2)$. From the scaling invariance, the $P_{\text{ext}}/P_{\text{contact}}$ ratio should not depend from the grain size, supposing same grain's shape for all sizes. Then we have $r_c/d \approx (P_{\text{ext}}/4P_{\text{contact}})^{1/2} = \text{const}$.
[30] A. R. Maxworty and E. McClelland, Geophys. J. Int. **140**, 101 (2000), and references therein.
[31] Y. Xu, D. Ephron, and M. R. Beasley, Phys. Rev. B **52**, 2843 (1995).
[32] A. Kozlowski, R. J. Rasmussen, J. E. Sabol, P. Metcalf, and J. M. Honig, Phys. Rev. B **48**, 2057 (1993).
[33] H. H. Kung, H. S. Jarrett, A. W. Sleight, and A. Feffetti, J. Appl. Phys. **48**, 2463 (1977).
[34] J. M. Daniels and A. Rosencwaig, J. Phys. Chem. Solids **30**, 1561 (1969).
[35] J. Tang, L. Feng, and J. A. Wiemann, Appl. Phys. Lett. **74**, 2522 (1999).
[36] N. F. Mott, *Metal-Insulator Transitions* (Taylor & Francis, New York, 1974).
[37] M. Viret, L. Ranno, and J. M. D. Coey, Phys. Rev. B **55**, 8067 (1997).
[38] L. G. Antoshina, A. N. Goryaga, and A. I. Kokorev, J. Magn. Magn. Mater. **258–259**, 516 (2003).
[39] J. P. Jakubovics, A. J. Lapworth, and T. W. Jolly, J. Appl. Phys. **49**, 2002 (1978).
[40] W. Rave, K. Ramstock, and A. Hulbert, J. Magn. Magn. Mater. **183**, 329 (1998).
[41] R. Aragon, Phys. Rev. B **46**, 5328 (1992).
[42] C. M. Srivastava and R. Aiyar, J. Phys. C **20**, 1119 (1987).
[43] E. De Grave, R. M. Persoons, R. E. Vandenberghe, and P. M. A. de Bakker, Phys. Rev. B **47**, 5881 (1993).
[44] H. Zijstra, IEEE Trans. Magn. **15**, 1246 (1979).
[45] In the limit of large conductive spots separated by thin resistive borders, the total potential distribution within intergrain contact is still close to the Maxwell approximation. In the opposite limit of scattered conductive spots, the Maxwell approximation is applied to each spot, and the resulted potential distribution at GB is consistent with high GB resistance. The subsequent analysis of spin-scattering mechanisms shows that an absolute spin resistance in TL is not very high for the moderate temperatures. That makes the above condition less important.
[46] P. Allia, M. Coisson, V. Selvaggini, P. Tiberto, and F. Vinai, J. Magn. Magn. Mater. **262**, 39 (2003).
[47] D. Ihle and B. Lorenz, J. Phys. C **18**, L647 (1985); **19**, 5239 (1986).
[48] J.-H. Park, L. H. Tjeng, J. W. Allen, P. Metcalf, and C. T. Chen, Phys. Rev. B **55**, 12813 (1997).
[49] H. Boppart, A. Schlegel, and P. Wachter, Philos. Mag. B **42**, 431 (1980); S. K. Park, T. Ishikawa, and Y. Tokura, Phys. Rev. B **58**, 3717 (1998).
[50] H. A. Alperin, O. Steinsvoll, R. Nathans, and G. Shirane, Phys. Rev. **154**, 508 (1967).
[51] P. M. Levy and S. Zang, Phys. Rev. Lett. **79**, 5110 (1997).
[52] V. Yu. Irkin and M. I. Katsnelson, Eur. Phys. J. B **30**, 481 (2002); V. Yu. Irkin and M. I. Katsnelson, Sov. Phys. Usp. **37**, 659 (1994).
[53] L. Degiorgi, P. Wachter, and D. Ihle, Phys. Rev. B **35**, 9259 (1987).
[54] J. Mannhart and H. Hilgenkamp, Mater. Sci. Eng., B **56**, 77 (1998).
[55] E. Y. Tsymbal and D. G. Pettifor, Phys. Rev. B **58**, 432 (1998).
[56] S. Lee, H. Y. Hwang, B. I. Shraiman, W. D. Ratcliff, II, and S. W. Cheong, Phys. Rev. Lett. **82**, 4508 (1999).
[57] S. Chikazumi, *Physics of Ferromagnetism* (Clarendon Press, Oxford, 1997).
[58] P. Bruno, Phys. Rev. Lett. **83**, 2425 (1999).